Sensitivity analysis of a Lorentz force flowmeter for laminar and turbulent flows in a circular pipe

By A. Thess†, B. Knaepen‡, E. Votyakov† AND O. Zikanov¶

We analyze the sensitivity of a Lorentz force flowmeter for two specific cases: a pipe flow exposed to a longitudinal magnetic field, and a pipe flow under the influence of a transverse magnetic field. The investigation involves both analytical solutions for laminar unidirectional flow and numerical solutions for turbulent flows. Our results show that the sensitivity of a Lorentz force flowmeter depends only weakly on the details of the mean velocity distribution. Also, the numerical simulations indicate that the kinematic theory performs quite well and that turbulent fluctuations do not strongly affect the measurements of the flowmeter. Furthermore, it is shown that the contribution of the fluctuations can be easily filtered out from the main flowmeter signal.

1. Introduction

A Lorentz force flowmeter is a device for the contactless measurement of flow rates in electrically conducting fluids. It measures the force on a magnet system that acts upon the flow, and has a wide variety of potential applications in metallurgy, semiconductor crystal growth, and glassmaking. This technique was originally proposed by Shercliff (1962) but has only recently been successfully implemented (Bucenieks 2005, Sjörström & Kelvesjö 2005, Thess *et al.* 2006) thanks to the advent of powerful rare-earth permanent magnets and sufficiently accurate force measurement systems. The goal of the present work is to analyze the sensitivity of a Lorentz force flowmeter using two specific simplified examples (shown in Fig. 1).

Generally, a Lorentz force flowmeter consists of a magnet system (either an electromagnet or a permanent magnet) that produces a primary magnetic field that acts upon the flow of an electrically conducting fluid. The currents that produce the primary field are called primary currents. Due to the flow under the influence of the primary magnetic field, eddy currents (also called secondary currents) are induced in the fluid (see Fig. 1 (a) and (c)). These currents interact with the primary magnetic field and produce a Lorentz force that brakes the flow. Due to Newton's law, a reciprocal force must therefore act on the magnet system whose measurement is the key ingredient of a Lorentz force flowmeter.

In order to successfully develop Lorentz force flowmeters, the following question needs to be answered: Given a primary magnetic field and a velocity field, what is the force acting on the magnet system? We will address this question in the framework of the *kinematic theory* in which we assume that the velocity field is given. We will analyze two specific flowmeters. The longitudinal flux flowmeter, to be examined in Section 2,

† Ilmenau University of Technology, Germany
‡ Université Libre de Bruxelles, Belgium
¶ University of Michigan - Dearborn, USA

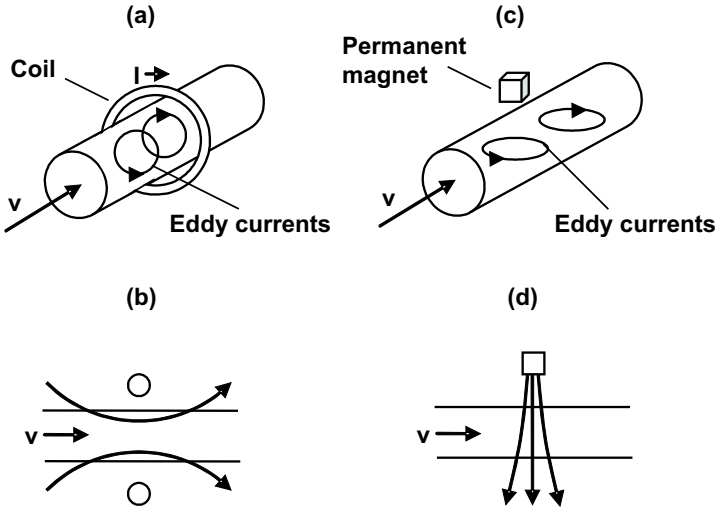

FIGURE 1. Sketch of the two problems considered: Longitudinal flux flowmeter (a), (b) and transverse flux flowmeter (c), (d). The shape of the primary magnetic field is shown in (b) and (d).

is characterized by the fact that the eddy currents are purely azimuthal and there is no need to calculate the electric potential as long as the flow is laminar and unidirectional. In Section 3 we examine the case of a transverse flux flowmeter; this discussion includes a computation of the eddy currents.

2. Longitudinal flux flowmeter

2.1. *Steady flow*

Our analysis begins with the case of a unidirectional flow of a fluid with electrical conductivity σ in a circular pipe with radius R that is subjected to an axisymmetric magnetic field given by

$$\mathbf{B} = B_r(r,z)\mathbf{e}_r + B_z(r,z)\mathbf{e}_z. \tag{2.1}$$

We use cylindrical coordinates (r,φ,z) with the unit vectors $\mathbf{e}_r$, $\mathbf{e}_\varphi$, and $\mathbf{e}_z$, where the coordinate z points in the streamwise direction. The magnetic field (2.1) has to satisfy the condition $\nabla\cdot\mathbf{B}=0$, but can otherwise be arbitrary. Flowmeters whose magnetic field is axisymmetric and whose symmetry axis coincides with that of the pipe will be called longitudinal flux flowmeters. We consider steady flows of the form

$$\mathbf{v} = v(r)\mathbf{e}_z. \tag{2.2}$$

To compute the Lorentz force in the framework of the kinematic theory we start with Ohm's law:

$$\mathbf{J} = \sigma(\mathbf{E} + \mathbf{v}\times\mathbf{B}). \tag{2.3}$$

In the case of low magnetic Reynolds numbers we can use the primary field given by Eq. (2.1) instead of the full magnetic field, and represent the electric field using an electric

potential $\mathbf{E} = -\nabla\Phi$. Taking the divergence of Ohm's law we obtain

$$\nabla^2\Phi = \mathbf{B}\cdot\omega, \tag{2.4}$$

where $\omega = \nabla\times\mathbf{v}$ is the vorticity. For flows of the form (2.2) the vorticity is parallel to $\mathbf{e}_\varphi$ so the right-hand side of (2.4) vanishes. Since the electric potential has to satisfy the homogeneous boundary conditions $\Phi = 0$ at $r = 0$ and $\partial\Phi/\partial r = 0$ at $r = R$, we have $\Phi = 0$, i.e., the potential vanishes. We can therefore immediately obtain the eddy currents

$$\mathbf{J} = \sigma v(r) B_r(r,z)\mathbf{e}_\varphi, \tag{2.5}$$

that are purely azimuthal and parallel to the wall of the pipe. The Lorentz force density acting on the fluid is given by

$$\mathbf{f} = \mathbf{J}\times\mathbf{B}. \tag{2.6}$$

We are only interested in the z-component of the total Lorentz force whose value will be denoted by F and is obtained by integrating the z-component of $\mathbf{f}$ over the volume of the pipe. The resulting expression reads

$$F = -2\pi\sigma\int_{-\infty}^{+\infty}\int_0^R v(r)B_r^2(r,z)\,r\,dr dz. \tag{2.7}$$

Since B_r^2 is positive, the force is always directed opposite to the flow, provided that $v(r)\geq 0$ everywhere (i.e., F and the volume flux $\int vrdr$ have opposite signs).

The force can be evaluated explicitly if the magnetic field has the form

$$B_r = \frac{3B_0}{2L^2}\,\frac{rz}{(1+z^2/L^2)^{5/2}}, \qquad B_z = B_0\,\frac{1}{(1+z^2/L^2)^{3/2}}. \tag{2.8}$$

This expression describes the magnetic field produced by a single coil with radius L wrapped around the pipe for the special case $R \ll L$ (see, e.g., Jackson 1975). The field has its maximum B_0 on the axis of the cylinder at $z = 0$. The integration over the magnetic field can be performed analytically and the total Lorentz force becomes

$$F = -\frac{45\pi^2}{256}\,\frac{\sigma B_0^2}{L}\int_0^R v(r)\,r^3\,dr. \tag{2.9}$$

This equation shows that the force on the longitudinal flux flowmeter depends on the shape of the velocity profile; furthermore, the flowmeter samples preferentially the velocity close to the wall. In order to determine how strongly the force depends on the shape of the velocity profile, let us analyze this expression for some particular cases. The velocity profile can conveniently be expressed as $v(r) = v_0 g(r/R)$ with a non-dimensional shape function $g(\xi)$, whose normalization $\int g(\xi)\xi d\xi = 1/2$ is such that the volume flux through the pipe equals $\pi R^2 v_0$, thus giving the velocity scale v_0 the meaning of the average velocity. The force can then be expressed as

$$F = -\frac{45\pi^2}{256}\,\frac{\sigma v_0 B_0^2 R^4}{L}\,S, \tag{2.10}$$

where the quantity

$$S = \int_0^1 g(\xi)\,\xi^3\,d\xi \tag{2.11}$$

can be interpreted as the sensitivity of the flowmeter.

The simplest case pertains to solid body translation for which $v(r) = v_0$ and thus

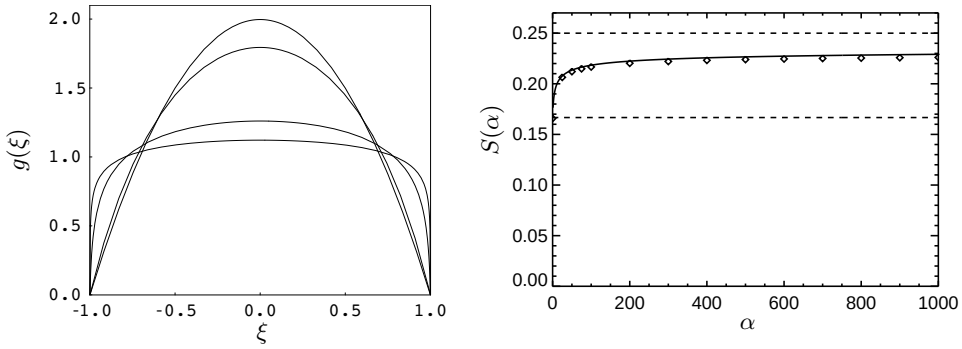

FIGURE 2. Sensitivity of the longitudinal flux flow meter: (Left) model profiles given by Eq. (2.14) and (right) sensitivity $S(\alpha)$ according to Eq. (2.15). The model profiles are plotted for $\alpha = 10^{-2}, 10^{0}, 10^{2}, 10^{4}$ (from top to bottom). The diamonds (right) represent the sensitivity computed numerically with the CDP code (see Section 2.2 for details).

$g(\xi) = 1$, which gives

$$S = \frac{1}{4}. \tag{2.12}$$

Considered next is the Poiseuille flow, which is described by $g(\xi) = 2(1 - \xi^2)$. After a straightforward integration we obtain

$$S = \frac{1}{6}, \tag{2.13}$$

which shows that the force from a Poiseuille flow is by a factor 2/3 smaller than for a moving solid body.

Let us now analyze the more general one-parameter family of profiles

$$g(\xi) = \beta(\alpha) \ln[1 + \alpha(1 - \xi^2)] \tag{2.14}$$

with $\beta(\alpha) = \alpha/[(1 + \alpha)\ln(1 + \alpha) - \alpha]$ to ensure the normalization $\int g(\xi)\xi d\xi = 1/2$. For $\alpha \to 0$ this profile obeys $g(\xi) \to 2(1 - \xi^2)$, i.e., it is Poiseuille-shaped, whereas for $\alpha \to \infty$ we have $g(\xi) \to 1$ as for solid body translation except for $\xi = 1$ where $g = 0$. Moreover, for $\alpha \gg 1$ this profile has the virtue of approximating the velocity distribution of a turbulent pipe flow where α is proportional to the Reynolds number (details below). Using symbolic integration it is straightforward to obtain the expression

$$S(\alpha) = \frac{2(1 + \alpha)^2 \ln(1 + \alpha) - \alpha(2 + 3\alpha)}{8\alpha[(1 + \alpha)\ln(1 + \alpha) - \alpha]} \tag{2.15}$$

for the sensitivity (one easily verifies that $S \to 1/6$ for $\alpha \to 0$ and $S \to 1/4$ for $\alpha \to \infty$, as obtained previously). Figure 2 shows that $S(\alpha)$ smoothly connects the limiting cases of Poiseuille flow and solid body translation.

Although the force on the Lorentz force flowmeter depends on the shape of the profile, the following numerical example shows that this dependence is weak. For turbulent flows the parameter appearing in the model profile (2.14) can be approximately identified with the Reynolds number $Re = 2Rv_0/\nu$ via $\alpha = \kappa(\lambda/2)^{1/2}Re$, where $\kappa = 0.41$ (Schade & Kunz 1989) is the von-Karman constant and the friction factor λ is a solution of Prandtl's universal equation $\lambda^{-1/2} = 2.0 \log[Re\,\lambda^{1/2}] - 0.8$. For a discussion of the coefficients in light of recent experiments, see Zagarola & Smits 1998. Let us compare the sensitivities

for $Re = 10^5$ and $Re = 10^6$, which represent typical values in metallurgy. For $Re = 10^5$ we have $\lambda = 0.01799$, $\alpha = 3889$, and $S = 0.2329$; for $Re = 10^6$ we obtain $\lambda = 0.01165$, $\alpha = 31290$, and $S = 0.2366$. Thus the sensitivities differ by only 2% when the Reynolds number changes by one order of magnitude.

2.2. *Unsteady flow*

The analytical computations of the previous section show that for a given flow rate ($\sim v_0$), the Lorentz force is rather insensitive to the actual averaged velocity profile (at least for typical values of the Reynolds number encountered in metallurgical applications). In this section we investigate the influence of turbulent fluctuations on the time signal of the Lorentz force. To that end, a numerical simulation of the pipe flow is performed using the finite volume code CDP developed at the Center for Turbulence Research (NASA Ames/Stanford Univ.) (Mahesh *et al.* 2004, Ham & Iaccarino 2004).

The pipe studied in this section has an aspect ratio of 10.0 (length/radius) and has been discretized using 101,648 elements. The flow is driven by a constant pressure gradient at an approximate Reynolds number $Re = 2v_0R/\nu = 3600$, where R is the radius of the pipe and ν is the viscosity of the fluid. For the longitudinal flux flowmeter, the magnetic field configuration is given by (2.8) with $L = 2$ (all numerical quantities quoted here are in SI units).

In order to first benchmark the MHD module developed for the CDP code and validate the analytical computations presented earlier, a first set of computations in which the velocity profile is *prescribed* to (2.14) is performed. The sensitivity function obtained in this fashion is displayed in fig. 2 (right) along with the analytical result (2.15). Note that for the longitudinal flux flowmeter, the numerically computed sensitivity lies within 1.5% of the analytical predictions for the whole range of parameter α explored. A similar validation of the MHD module for the transverse flux flowmeter is performed (see section 3) and shows that the sensitivity lies within 0.5% of the values computed analytically for that situation (fig. 7).

Two separate turbulent simulations were then performed (contrary to the previous two tests outlined in the preceding paragraph, the velocity field is now computed by true direct numerical simulation). The first case consists of a kinematic simulation in which the Lorentz force is computed from the velocity field but does not act on it. In the second simulation, the Lorentz force acts on the velocity field and therefore constitutes a complete MHD simulation of the flux flowmeter. For this run, the parameters are chosen in such a way that the interaction parameter, which measures the relative strength of the Lorentz force to inertial effects, is approximately equal to $N = (2\sigma B_0^2 R)/(\rho v_0) = 0.2$, where ρ is the density of the fluid. This value of N is typical of metallurgical applications.

As previously mentioned, in both runs, the flow is sustained using a constant pressure gradient and the instantaneous flow rate thus slowly varies with time (see Fig. 3 (left)). As expected, the mean velocity v_0 is slightly smaller in the MHD case since extra dissipation is introduced by the Lorentz force while the forcing is identical to that used in the kinematic case.

Also shown in fig. 3 (right) is the time history of the integrated Lorentz force. The plots clearly show that the oscillations present in the average velocity are reproduced in F. However, some fluctuations of much higher frequencies are also present. The origin of these rapid oscillations is easily understood when one recalls that in the case of the longitudinal flux flowmeter, the magnetic field is quite strongly localized in the vicinity of $z = 0$ and samples more intensively the near-wall structures (see also (2.9) and the r^3 dependence of the Lorentz force). Therefore, the Lorentz force varies rapidly as turbulent

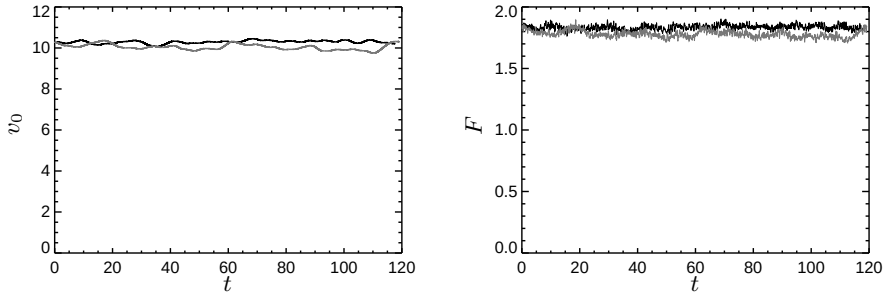

FIGURE 3. Time histories of (a) average velocity v_0 and (b) integrated Lorentz force F for the unsteady turbulent pipe and longitudinal flux flowmeter. Both plots contain the kinematic (dark line) and MHD (gray line) cases.

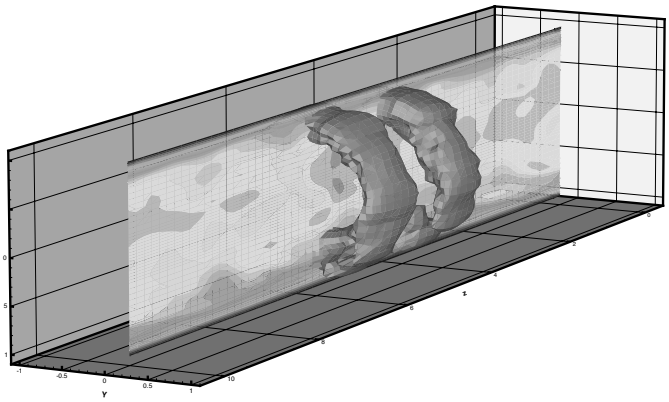

FIGURE 4. Iso-contour of the Lorentz force in the region of space where it is the strongest. The sliced plane contains a contour of the intensity of the velocity field in the streamwise direction.

eddies cross the "active" region of the flowmeter. To illustrate this point, we plot in Fig. 4 an iso-contour of the intensity of the Lorentz force for a given instantaneous velocity field; this iso-contour highlights the region of space where the Lorentz force is the strongest.

To study the relationship between the average velocity and the Lorentz force in greater detail, the spectra of the normalized time series contained in fig. 3 are shown in Fig. 5 (the kinematic case is considered first). Note that the signals have been normalized by removing their mean and dividing them by their standard deviations. Because of the limited sampling available, those spectra inevitably appear very noisy. Nevertheless, the figure indicates that both spectra are very similar at low wavenumbers, while the spectrum corresponding to the Lorentz force is significantly larger in the high wavenumber range.

Because of the similarity of the spectra at low wavenumbers, it is interesting to filter the normalized signals by retaining their Fourier modes up to a frequency at which the respective spectra appear to strongly deviate. This cutoff frequency is of course not well-defined but based on Fig. 5, the value $k = 50$ seems a reasonable choice. Those filtered normalized signals, respectively $\hat{v}_0(t)$ and $\hat{F}(t)$, are plotted in Fig. 6 (left) and do appear very similar, except that the time series for both appear to be time-shifted. This shift can be measured by computing the correlation of $\hat{v}_0(t)$ and $\hat{F}(t + \Delta t)$ as a function of

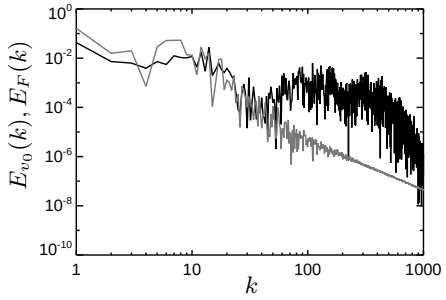

FIGURE 5. Spectra of the time series of the mean velocity (gray line) and integrated Lorentz force (dark line). Only the signals corresponding to the kinematic simulation are considered.

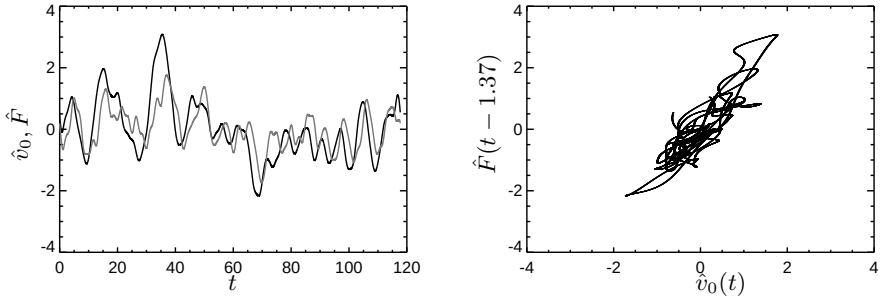

FIGURE 6. Left: time history of the low-pass filtered signals $\hat{v}_0$ (grey line) and $\hat{F}$ (dark line). Only the kinematic simulation is considered. Right: $\hat{F}(t-1.37)$ as a function of $\hat{v}_0(t)$ for the MHD simulation. The correlation of the two signals is $\mathcal{C} = 0.962$.

Δt and finding the maximum value. For the two signals shown in Fig. 6 the optimal value is $\Delta t = -1.15$; for this value of Δt, the correlation $\mathcal{C}$ between the velocity and the Lorentz force is $\mathcal{C} = 0.873$ (while it is equal to 0.69 for $\Delta t = 0$). This measurement thus confirms that the oscillations in the velocity average v_0 are preceded by corresponding low frequency oscillations in the Lorentz force measured. In the present case, the time shift is roughly equal to the crossing time of the flow through the pipe since $v_0 \sim 10$ and $L_{pipe} = 10$.

The same analysis can be performed for the MHD case. The spectra of the normalized signals $v_0(t)$ and $F(t)$ are again very similar at low frequencies and their low-pass versions look analogous except for a time shift. The maximum correlation here is observed for $\Delta t = -1.37$ and has a high value of $\mathcal{C} = 0.962$; for $\Delta t = 0$ the correlation is equal to 0.820. The high correlation of $\hat{v}_0(t)$ and $\hat{F}(t-1.37)$ is illustrated in Fig. 6 (right), where $\hat{F}$ is plotted as a function of $\hat{v}_0$.

3. Transverse flux flowmeter

It is often desirable to use magnetic systems that are located on only one side of the pipe and whose magnetic field is predominantly transverse to the direction of the mean flow. These systems are called transverse flux flowmeters. Unlike longitudinal flux flowmeters, which encircle the flow entirely, the transverse flux flowmeters do not have to be disassembled and reassembled for use in different locations.

To develop a general understanding of the main characteristics of transverse flux flowmeters we consider a steady unidirectional pipe flow with the same general velocity profile (Eq. (2.2)) as discussed in the previous section. Our purpose is to investigate the effect of two-dimensional magnetic fields of the form

$$\mathbf{B} = B_y(y,z)\mathbf{e}_y + B_z(y,z)\mathbf{e}_z. \tag{3.1}$$

Here $x = r\cos\varphi$ and $y = r\sin\varphi$ are Cartesian coordinates that will be used in addition to the cylindrical coordinates introduced in the previous section. The components of the magnetic field must satisfy the condition $\partial B_y/\partial y + \partial B_z/\partial z = 0$, but can otherwise be arbitrary. We are interested in the streamwise component of the Lorentz force that is not affected by B_z. We therefore only need to prescribe the transverse component B_y.

For simplicity, we assume that the variation of this quantity over the cross section of the pipe $-R \le y \le +R$ is weak, in which case the dependence of B_y on y can be neglected. This corresponds to the situation in which the distance between the source of the magnetic field and the pipe is much larger than the diameter of the pipe. Hence we can write $B_y(y,z) \approx B(z)$ inside the pipe. Knowing that any distribution $B(z)$ can be expanded into a Fourier series, it is natural to start with the simplest case,

$$B(z) = B_0 \cos kz, \tag{3.2}$$

which is the simplest model describing the spatially periodic distribution of the magnetic field in a rotary flowmeter.

In the present case the electric potential does no longer vanish; it has to be obtained by solving Eq. (2.4)

$$\nabla^2\Phi = -B_0 \cos kz \cos\varphi \frac{dv}{dr}, \tag{3.3}$$

with the boundary conditions

$$\Phi = 0 \ (\text{for } r = 0), \qquad \frac{\partial\Phi}{\partial r} = 0 \ (\text{for } r = R). \tag{3.4}$$

The first boundary condition ensures that the electric potential is unique and the electric current is non-singular at the origin, whereas the second boundary condition expresses that the normal component of the electric current vanishes at the wall, which we assume to be electrically insulating. Note that the second condition is valid only if the flow satisfies the no-slip condition at the wall. In other cases, for example, in the case of solid-body translation considered below, the condition has to be modified to

$$\frac{\partial\Phi}{\partial r} = (\mathbf{u}\times\mathbf{B})_r \ (\text{for } r = R). \tag{3.5}$$

The solution of (3.3) can be represented as

$$\Phi(r,\varphi,z) = -v_0 B_0 R \cos kz \cos\varphi \cdot f\left(\frac{r}{R}\right), \tag{3.6}$$

where $f(\xi)$ is a solution of the equation

$$\xi^2 f'' + \xi f' - (\kappa^2\xi^2 + 1)f = \xi^2 g'(\xi) \tag{3.7}$$

with the boundary conditions $f(0) = 0$ and $f'(1) = 0$. In (3.7), $g(\xi)$ is the shape function of the velocity profile defined in the previous section and $\kappa = kR$ is the non-dimensional wavenumber of the magnetic field. Once this equation has been solved, the Lorentz force density

$$\mathbf{F} = \sigma(-\nabla\Phi + \mathbf{v}\times\mathbf{B})\times\mathbf{B} \tag{3.8}$$

can be evaluated. As in the previous section, we are only interested in the z-component of the Lorentz force. Inserting (3.6) into (3.8) and integrating over the volume $\pi R^2 L$ of one period of the magnetic field (where $L = 2\pi/k$), we obtain the total force as

$$F = -\frac{\pi}{2}\,\sigma v_0 B_0^2 R^2 L\, S(\kappa). \tag{3.9}$$

Here the sensitivity is given by

$$S(\kappa) = 1 - f(1). \tag{3.10}$$

This relation shows that we only need to know the non-dimensional potential $f(1)$ at the wall of the pipe in order to compute S. In contrast to the case considered in the previous section, the sensitivity depends not only on the shape of the velocity profile, but also on the wavenumber κ of the magnetic field.

As in the previous section, we analyze the dependency of the force field (3.9) on the velocity profile. In the case of solid-body translation, the right-hand side of (3.7) is zero and the equation reduces to the modified Bessel equation. Since the no-slip condition is violated by such a flow, the boundary condition at $\xi = 1$ changes to $f'(1) = 1$ (see (3.5)). The solution and the sensitivity function (3.10) can be computed in terms of the modified Bessel functions

$$f(\xi) = \frac{I_1(\kappa\xi)}{\kappa I_1'(\kappa)}, \quad S(\kappa) = \frac{\kappa I_0(\kappa) - 2I_1(\kappa)}{\kappa I_1'(\kappa)}, \tag{3.11}$$

where $\kappa I_1'(\kappa) = \kappa dI_1(\kappa)/d\kappa = \kappa I_0(\kappa) - I_1(\kappa)$. In the case of a laminar pipe Poiseuille flow with $g(\xi) = 2(1-\xi^2)$ Eq. (3.7) with homogeneous boundary conditions can be solved analytically as

$$f(\xi) = -\frac{4I_1(\kappa\xi)}{\kappa^3 I_1'(\kappa)} + \frac{4\xi}{\kappa^2}, \quad S(\kappa) = 1 + \frac{4I_1(\kappa)}{\kappa^3 I_1'(\kappa)} - \frac{4}{\kappa^2}. \tag{3.12}$$

As reported in Section 2.2, this solution was verified against numerical results obtained by the CDP code (see Fig. 7).

No analytical solution could be found for the case of the more general one-parameter velocity profile (2.14), so we used numerical integration. The boundary-value problem was solved using a shooting procedure based on the adaptive step-size Runge-Kutta algorithm of predetermined solution accuracy. Asymptotic expansion was used to treat the singular point at $\xi = 0$.

The results are presented in Fig. 7. As was the case with the longitudinal flowmeter results, the measured force is weakly affected by the details of the flowfield. Vastly different velocity profiles illustrated in Fig. 2 generate only slightly different sensitivity functions.

In addition to the total Lorentz force, of interested is the mean Lorentz force density $f = F/(\pi R^2 L)$, which is equal to

$$f = \frac{1}{2}\,\sigma v_0 B_0^2\, S(\kappa). \tag{3.13}$$

Figure 7 shows that the sensitivity of the flowmeter is a monotonically increasing function of the wavenumber. For small wavenumbers the magnetic field depends only weakly on z; the eddy currents are predominantly in the x–y plane and their contribution to the force is small. As the wavenumber grows the eddy currents become more and more three-dimensional and the Lorentz force increases. However, conclusions about the monotonic nature of $S(\kappa)$ should take into account that, in practice, the magnetic field amplitude B_0 is not a constant. Specifically, assume that the magnetic field (3.2) was

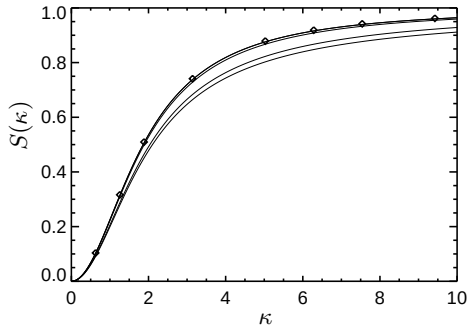

FIGURE 7. Sensitivity of the transverse fluxflow meter: Sensitivity function $S(\kappa)$ plotted as a function of κ for the parabolic Poiseuille profile, generalized profiles (2.14) with $\alpha = 10^0, 10^2, 10^4$, and solid-body translation (from top to bottom); the diamonds represent the sensitivity function of the parabolic profile computed numerically using the CDP code (see Section 2.2). Note that the sensitivity function obtained at $\alpha = 10^{-2}$ is indistinguishable from the function for the parabolic profile.

produced by a thin sheet of electric current with thickness δ located at a distance D below the pipe, whose current density is given by $\mathbf{J} = J_0 \sin(kz)\mathbf{e}_x$ (for $-D - \delta/2 \le y \le -D + \delta/2$) and $\mathbf{J} = 0$ elsewhere. In the limit $k\delta \to 0$ (very thin sheet) the transverse magnetic field produced by the sheet is

$$B_y(y, z) = \mu_0 J_0 \delta e^{-k|y-D|} \cos kz. \tag{3.14}$$

If we further assume that the power consumption for producing the electric current, expressed in terms of dissipated Joule heat per unit length $q = (J_0^2/\sigma) \cdot 2\pi\delta/k$ is prescribed, we can write the current density as $J_0 = (\sigma k q/2\pi\delta)^{1/2}$ and the amplitude of the magnetic field becomes

$$B_0^2 = \frac{\mu_0^2 \sigma q \delta}{2\pi} k\, e^{-2kD}. \tag{3.15}$$

This relation shows that the magnetic field amplitude decreases exponentially for large wavenumbers, so for a given electric power q (per unit length) the Lorentz force has a maximum at a certain finite value of κ. This example demonstrates the importantance of properly considering the source of the magnetic field.

4. Summary and conclusions

We have established the theoretical foundations of Lorentz force velocimetry by computing the force acting on a magnet system that interacts with a liquid metal flow in a circular pipe. The most important results of the present analysis and simulations are (1) the weak dependence of the force on the details of the velocity profile and (2) the suitability of a purely kinematic approach. Further studies will focus on more realistic magnetic field distributions and other types of fluid flow.

Acknowledgments

The authors are grateful to Prof. Parviz Moin and the staff of the Center for Turbulence Research for their hospitality during the 2006 Summer Program. We are particularly

grateful to Prof. Gianluca Iaccarino, Dr. Frank Ham and Prof. Stavros Kassinos for their invaluable help with the numerical simulations and for the opportunity to use the CDP simulation software.

AT and EV acknowledge support from the Deutsche Forschungsgemeinschaft in the framework of the "Forschergruppe Magnetofluiddynamik" at the Technische Univesität Ilmenau, and also thank Y. Kolesnikov for useful discussions.

OZ acknowledges support from the U.S. Department of Energy (Grant DE FG02 03 ER46062). The cooperation between the University of Michigan - Dearborn and Ilmenau University of Technology is supported by the U.S. National Science Foundation (Grant INT 0338713).

This work, conducted as part of the award "B. Knaepen – Modelling and simulation of turbulent conductive flows in the limit of low magnetic Reynolds number" made under the European Heads of Research Councils and European Science Foundation EURYI (European Young Investigator) Awards scheme, was supported by funds from the Participating Organisations of EURYI and the EC Sixth Framework Programme.

REFERENCES

Bucenieks I. 2005 Modelling of rotary inductive electromagnetic flowmeter for liquid metals flow control. *Proceedings of the 8th International Symposium on Magnetic Suspension Technology,* September 26 28, 2005, Dresden, Germany, Editors: G. Fuchs, L. Schultz, O. de Haas H.-J. Schneider-Muntau, 204–208.

Ham F., Iaccarino G. 2004 Energy conservation in colocated discretization schemes on unstructured meshes. *Annual Research Briefs 2004*, Center For Turbulence Research, NASA Ames/Stanford Univ.

Jackson J.D. 1975 Classical Electrodynamics. Wiley, New York.

Mahesh K., Constantinescu G., Moin P. 2004 A numerical method for large-eddy simulation in complex geometries. *J. Comp. Phys.* **197**.

Schade H., Kunz E. 1989 Strömungslehre, 2nd edition, Walter de Gruyter, Berlin, New York, Chapter 13.5 (in German).

Sjörström U., Kelvesjö H. 2005 Sensor for non-contact velocity measurements for continuous casting slab moulds - first results from industrial measurements. *Proceedings Continuous Casting Conference*, Nice, France.

Shercliff J.A. 1962 The Theory of Electromagnetic Flow Measurement. *Cambridge University Press.*

Thess, A., Votyakov E., Kolesnikov, Y. 2006 Lorentz force velocimetry. *Phys. Rev. Lett.*, **96**, 164501.

Zagarola M.J., A.J. Smits 1998 Mean-flow scaling of turbulent pipe flow. *J. Fluid Mech.*, **373**, 33–79.